J Mater Sci: Mater Electron (2016) 27:9962–9975
DOI 10.1007/s10854-016-5067-3

Photo-degradation of azo dyes: photo catalyst and magnetic investigation of $CuFe_2O_4$–TiO_2 nanoparticles and nanocomposites

Shamin Masoumi[1] · Gholamreza Nabiyouni[1] · Davood Ghanbari[2]

Received: 5 March 2016 / Accepted: 23 May 2016 / Published online: 3 June 2016

Abstract $CuFe_2O_4$ nanoparticles were first synthesized via a fast and simple precipitation method. Then $CuFe_2O_4$–TiO_2 nanocomposites were prepared using sol–gel method. The prepared products were characterized by X-ray diffraction, scanning electron microscopy, and fourier transform infrared spectroscopy. Alternating gradient force magnetometer was used to study the magnetic property of the products. The results illustrated either superparamagnetic or ferromagnetic behaviour of $CuFe_2O_4$ nanoparticles. The photo-catalytic behaviour of $CuFe_2O_4$–TiO_2 nanocomposites was evaluated using the degradation of four various azo dyes under ultraviolet light irradiation. The results show that the prepared nanocomposites are applicable for magnetic and photo-catalytic performance.

1 Introduction

Nano crystalline ferrites with the general formula MFe_2O_4 (M refers to Co, Ni, Cu, Zn,…) are very important magnetic materials because of their interesting magnetic and electrical properties with chemical and thermal stabilities. The ferrite materials may be classified into three different classes, spinel, garnet, and hexagonal ferrites. Nano ferrites are used in several industries e.g. magnetic recording and data storage technology, radar absorbing and magneto-electric technologies. Ferrites have been used as active catalysts in various reactions, for example, as hydrocarbon oxidation, decomposition of alcohols, oxidative dehydrogenation, and peroxides and decarboxylation, electro-catalytic activity and corrosion resist. Transition metal ferrites constitute an important class of spinel oxides that exhibit a broad range of interesting physical properties [1–3]. Magnetic separation is considered as a high speed and effective technique for separating magnetic particles. Thus, if the powder adsorbent catalyst is magnetic, it could be recovered conveniently by magnetic field [4, 5]. Ferrites, being important class of magnetic materials have also been utilized as catalysts for nitro reduction and nitro-phenol reduction [6]. Ferrites are receiving increased attention due to their applications in preparation of high density ferrite cores, adsorbents, suspension materials in ferromagnetic liquids, catalysts CO_2 decomposition reaction, the cross-coupling of terminal alkynes or thiols, refractory materials, super-hard materials and high temperature sensors. The ultrafine particles of ferrites are found to alter the electro-optical, various applications in hydrogen production, lithium on batteries, high density magneto-optic recording devices, magnetic refrigeration and ferrofluids [7–9]. Among them copper ferrites are very important and have been widely used in the electronic industries. $CuFe_2O_4$ is known to exist in tetragonal and cubic structures according to their preparation conditions. The tetragonal structure is stable at room temperature and transforms to cubic phase at temperatures above 623 °K due to Jahn–Teller distortion. This distortion is directly related to the magnetic properties. The cubic structure possesses a larger magnetic moment than which of the tetragonal one, because there are more cupric ions (Cu^{2+}) at tetrahedral sites in cubic structure in comparison to the tetragonal structure. The cubic cell parameter is $a = 8.37$ Å, while the tetragonal unit cell has lattice parameters of $a = 5.81$ Å and

✉ Gholamreza Nabiyouni
G-nabiyouni@araku.ac.ir

[1] Department of Physics, Faculty of Science, Arak University, Arak 38156-88349, Iran

[2] Young Researchers and Elite Club, Arak Branch, Islamic Azad University, Arak, Iran

Table 1 Precursors, precipitating agents, temperature and magnetic treatments

No	Precursors	Precipitating agent	Temp (°C)	Magnetic behaviour
1	$Cu(NO_3)_2{\cdot}3H_2O$, $Fe(NO_3)_3{\cdot}9H_2O$	NaOH	200	Superparamagnetic
2	$Cu(NO_3)_2{\cdot}3H_2O$, $Fe(NO_3)_3{\cdot}9H_2O$	NaOH	400	Superparamagnetic
3	$Cu(NO_3)_2{\cdot}3H_2O$, $Fe(NO_3)_3{\cdot}9H_2O$, SDS	NaOH	200	Superparamagnetic
4	$Cu(NO_3)_2{\cdot}3H_2O$, $Fe(NO_3)_3{\cdot}9H_2O$, SDS	NaOH	400	Ferromagnetic
5	$Cu(NO_3)_2{\cdot}3H_2O$, $Fe(NO_3)_3{\cdot}9H_2O$, PVA	NaOH	200	Superparamagnetic
6	$Cu(NO_3)_2{\cdot}3H_2O$, $Fe(NO_3)_3{\cdot}9H_2O$, PVA	NaOH	400	Ferromagnetic
7	$Cu(NO_3)_2{\cdot}3H_2O$, $Fe(NO_3)_3{\cdot}9H_2O$, PVA	NaOH	600	Ferromagnetic
8	$Cu(NO_3)_2{\cdot}3H_2O$, $Fe(NO_3)_3{\cdot}9H_2O$	NH_3	200	Superparamagnetic
9	$Cu(NO_3)_2{\cdot}3H_2O$, $Fe(NO_3)_3{\cdot}9H_2O$, PVA	NH_3	200	Superparamagnetic
10	$Cu(NO_3)_2{\cdot}3H_2O$, $Fe(NO_3)_3{\cdot}9H_2O$, SDS	NH_3	200	Superparamagnetic
11	TTIP, methanol, HNO_3, water	NaOH	500	Non-magnetic TiO_2
12	$CuFe_2O_4$–TiO_2	NaOH	500	Superparamagnetic

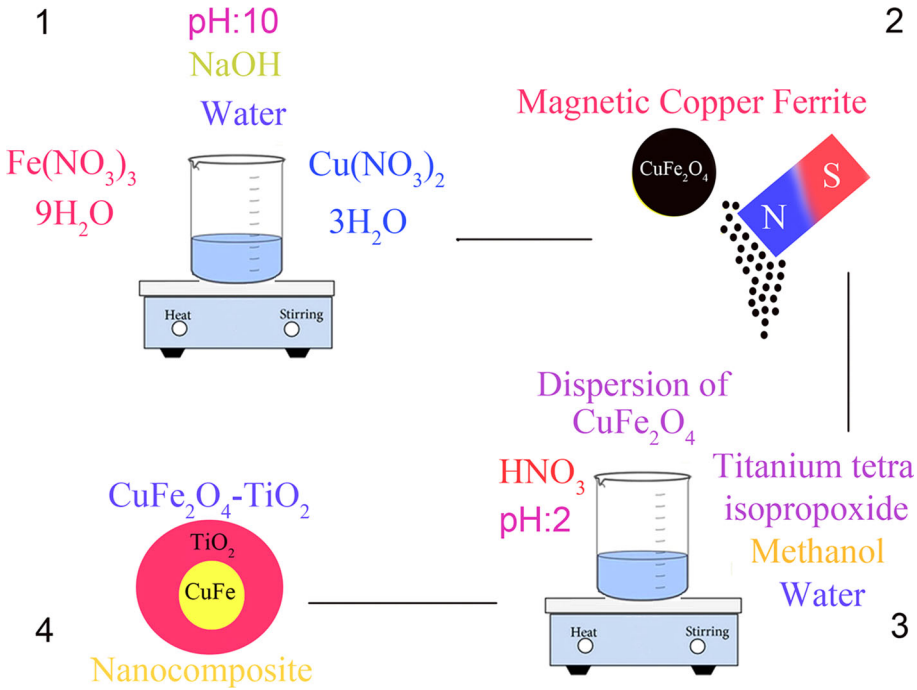

Fig. 1 Schematic of nanocomposite preparation

c = 8.71 Å (c/a = 1.50) [10, 11]. Due to the low migration energy of copper ions in the spinel lattice, copper ferrite in its bulk equilibrium form is a partial inverse spinel [12]. As a p-type semiconductor, $CuFe_2O_4$ has been considered to be a novel and promising catalyst for photo catalytic H_2 production under visible light irradiation. The two crystalline forms of $CuFe_2O_4$ show different catalytic activities, the tetragonal form is more active than the cubic form. Thus tetragonal $CuFe_2O_4$ is suitable for high catalytic activity [13–16]. $CuFe_2O_4$ is ferrimagnetic material with a Curie temperature around 500 °C [17]. Among diverse available methods ball-milling, sol–gel, co-precipitation and ceramic synthesis, are interesting and attract much research attention. In a co-precipitation procedure, the pH of a metal salt solution is raised by adding a base in order to precipitate the hydroxides; this requires a strict control of the pH and the stirring rate. The most widely used methods for the synthesis and control of the crystallite size of ferrites are sol–gel, co-precipitation and solid state methods. These methods yield the crystallites in the nanometer range (1–100 nm). TiO_2 are very promising visible light active photo catalysts that have been widely investigated for water purification and removal of different organic compounds from industrial wastewater [18–27].

In this work $CuFe_2O_4$ nanoparticles were first synthesized via a fast and simple precipitation method. $CuFe_2O_4$–TiO_2 nanocomposites were then synthesized by sol–gel method. The photo catalytic behaviour of $CuFe_2O_4$–TiO_2

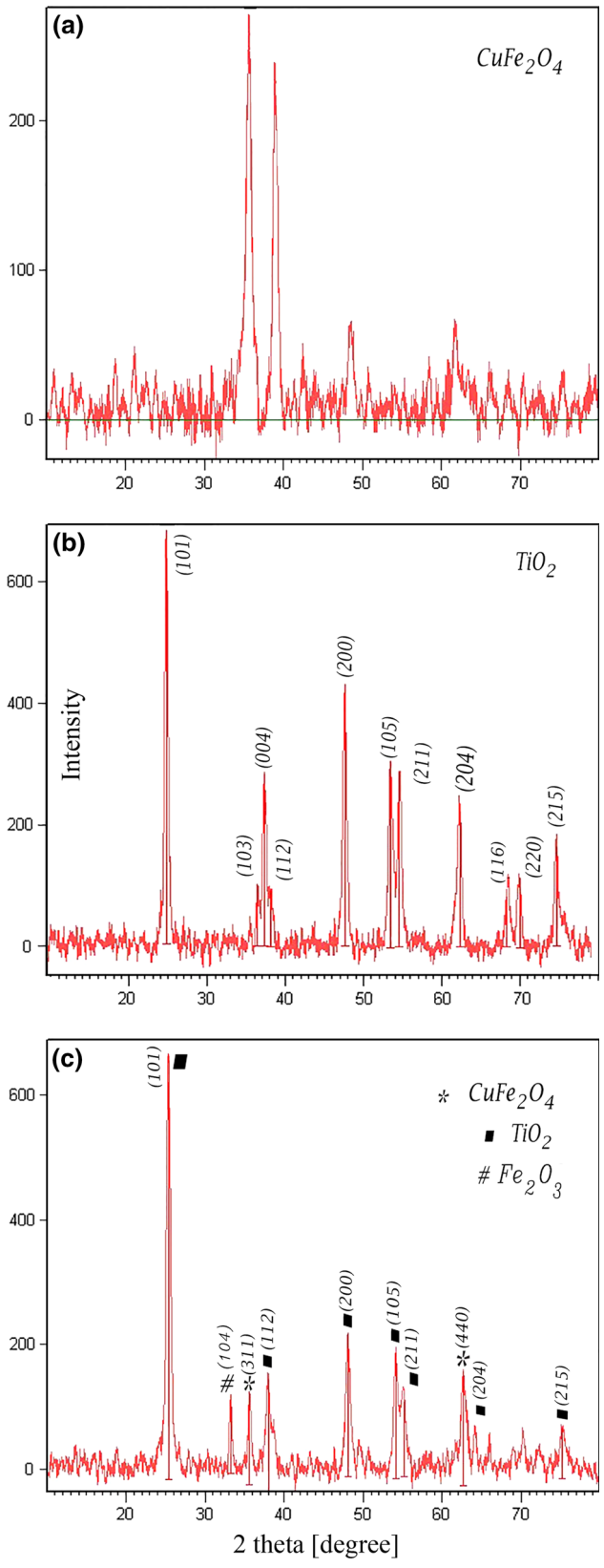

Fig. 2 XRD pattern of **a** $CuFe_2O_4$, **b** TiO_2 nanoparticle, **c** $CuFe_2O_4$–TiO_2 nanocomposite

nanocomposites was evaluated using the degradation of four various azo dyes under ultraviolet light irradiation. The results show that our synthesized nanocomposites have superparamagnetic or ferromagnetic behaviours and are applicable for photo-catalytic performance.

2 Experimental

2.1 Materials and methods

$Fe(NO_3)_3{\cdot}9H_2O$, $Cu(NO_3)_2{\cdot}3H_2O$, NaOH, NH_3, sodium dodecyl sulphate (SDS), polyvinyl alcohol MW: 170,000 (PVA), distilled water, titanium tetra isopropoxide (TTIP) and methanol were purchased from Merck Company. XRD patterns were recorded by a Philips, X-ray diffractometer using Ni-filtered CuK_α radiation. SEM images were obtained using a LEO instrument model 1455VP. All the chemicals were used as received without further purifications. Room temperature magnetic properties were investigated using an alternating gradient force magnetometer (AGFM and VSM) device, (Meghnatis Kavir Kashan Co., Iran) in an applied magnetic field sweeping between ±10,000 Oe. Prior to taking SEM images, the samples were coated by a very thin layer of Pt (using a BAL-TEC SCD 005 sputter coater) to make the sample surface conductor and prevent charge accumulation, and obtaining a better contrast. A multiwave ultrasonic generator (Bandeline MS 73), equipped with a converter/transducer and titanium oscillator, operating at 20 kHz with a maximum power output of 150 W was used for the ultrasonic irradiation.

2.2 Synthesis of $CuFe_2O_4$ nanoparticles

First 0.64 g of $Fe(NO_3)_3{\cdot}9H_2O$ and 0.2 g of $Cu(NO_3)_2{\cdot}3H_2O$ were dissolved in 100 ml of distilled water. 0.05 g of SDS or polyvinyl alcohol MW: 170,000 (PVA) was then added to the solution as surfactant, and it was mixed and heated at 80 °C on magnetic stirring for 20 min. Then 8 ml of NaOH (1M) was slowly added as precipitator the pH of solution and was fixed to 10. The obtained black precipitate was washed twice with distilled water. The product then was dried in oven for 24 h and was calcinated at 200, 400 and 600 °C for 2 h. Table 1 shows various precursors, precipitating agents, temperature and magnetic treatments. In other synthesis the above steps were repeated but 1 ml of ammonia was used as a precipitating agent, and the product was calcinated at 200 °C for 2 h.

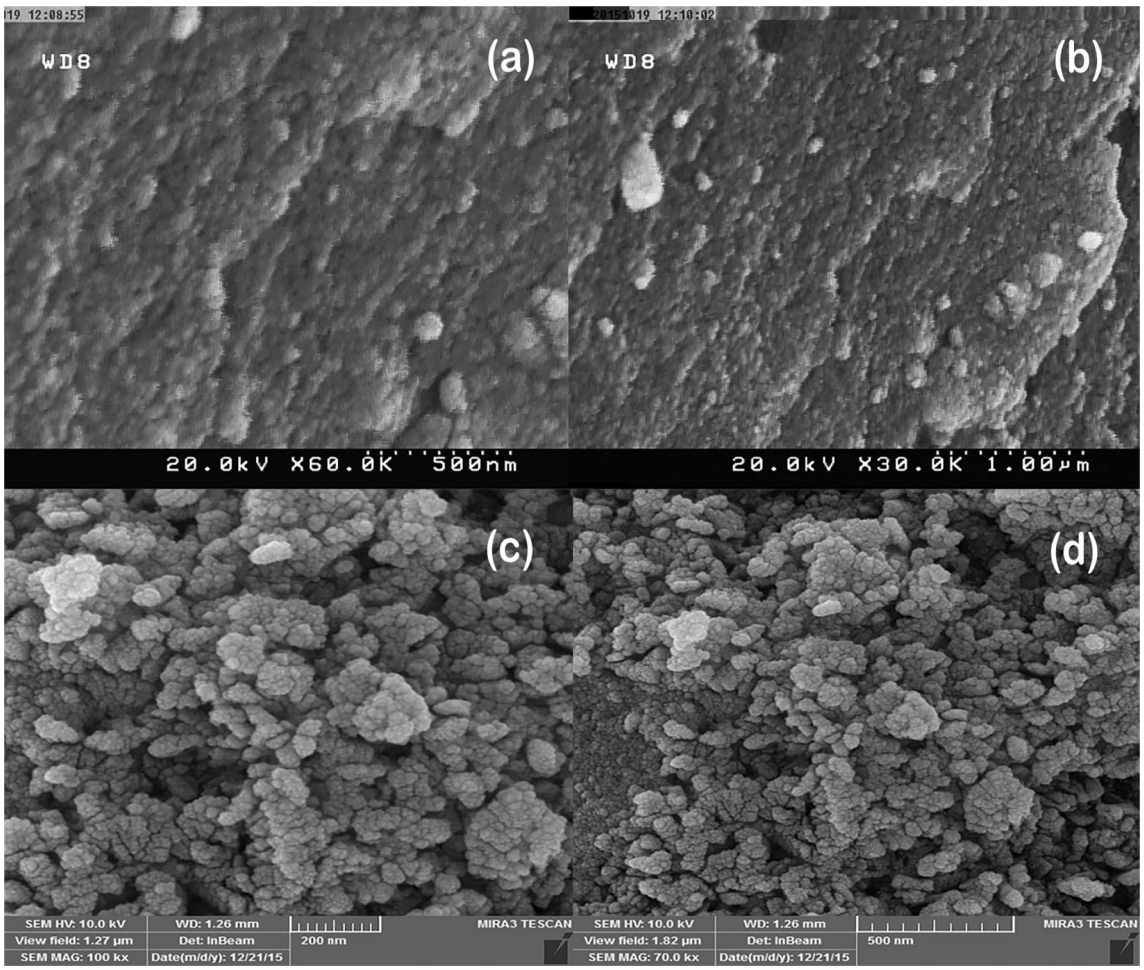

Fig. 3 SEM images of surfactant-free $CuFe_2O_4$ **a**, **b** 200 °C no. 1; **c**, **d** 400 °C no. 2

2.3 Synthesis of $CuFe_2O_4$–TiO_2 (50:50 %, 0.1:0.1 g) nanocomposites

Firstly 0.1 g of synthesized copper ferrite was dispersed in 10 ml of methanol. It was mixed on magnetic stirring for 15 min. Then 0.25 g of titanium tetra isopropoxide (TTIP) (Yield of TiO_2: 0.1 g) was added to the solution and was mixed for 10 min. After that 1 ml of distilled water was added and the solution was stirred for 10 min. HNO_3 was slowly added to reaching pH of solution to 2. After 90 min stirring the gel was obtained. Then it was dried in oven for 45 min and was calcinated at 500 °C for 2 h (Fig. 1).

2.4 Photo-catalytic degradation process

Ten milliliters of the dye solution (20 ppm) was used as a model pollutant to determine the photocatalytic activity. 0.1 g of catalyst was applied for degradation of 10 ml solution. The solution was mixed by a magnet stirrer for 1 h in darkness to determine the adsorption of the dye by catalyst and better availability of the surface. The solution was irradiated by a 100 W UV lamp which was placed in a quartz pipe in the middle of reactor. It was turned on after 1 h stirring the solution and sampling (about 10 ml) was done every 15 min. The samples were filtered, centrifuged and their concentration was determined by UV–visible spectrometry.

3 Results and discussion

Figure 2a illustrates XRD pattern of $CuFe_2O_4$ product. Cubic phase of ferrite (JCPDS No. 25-0283) can be observed in this pattern. The pattern confirms formation of copper ferrite with space group of Fd-3 m. Figure 2b shows XRD pattern of TiO_2 product. It can be observed that Anatase phase with JCPDS No. 21-1272 and space group of I41/amd is present in the pattern.

The composition of the $CuFe_2O_4$–TiO_2 nanocomposite was investigated by XRD pattern and it is depicted in

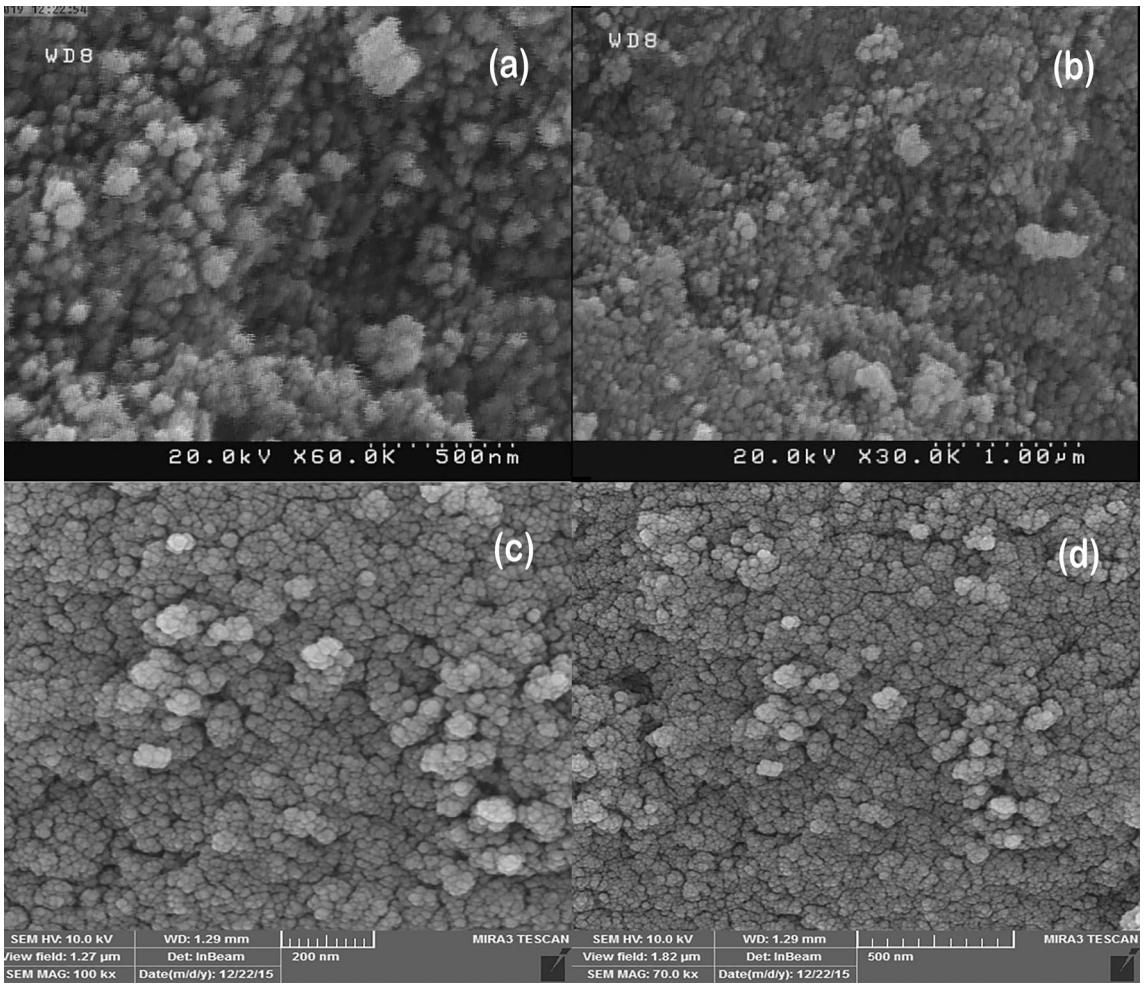

Fig. 4 SEM images of $CuFe_2O_4$ prepared by SDS **a**, **b** 200 °C no. 3; **c**, **d** 400 °C no. 4

Fig. 2c. It confirms presence of both phase of $CuFe_2O_4$ (JCPDS No. 25-0283) and Anatase phase of TiO_2 (JCPDS No. 21-1272) in the pattern. The peak intensities related to each counterpart is relatively similar which is representative of rather equal portion of the shared compounds in the composite. The crystalline sizes are calculated from Scherrer equation, $D_c = K\lambda/\beta Cos\theta$, where β is the width of the observed diffraction peak at its half maximum intensity (FWHM), K is the shape factor, which takes a value of about 0.9, and λ is the X-ray wavelength (CuK_α radiation, equals to 0.154 nm). The values of about 20 and 19 nm were found for crystalline sizes of $CuFe_2O_4$ and $CuFe_2O_4$–TiO_2 nanoparticles, respectively.

Effect of temperature on the morphology and particle size of products was investigated. Figure 3a, b illustrate SEM images (in two different magnifications) of as-synthesized $CuFe_2O_4$ nanoparticles, calcinated at 200 °C. The images indicate that the nanoparticles with average diameter size of less than 60 nm were prepared. Figure 3c, d show SEM images (in two magnifications) of the $CuFe_2O_4$ nanoparticles obtained at 400 °C and illustrate nanoparticles with mediocre diameter size of about 70 nm and it seems the nucleation was preferential compare to the crystal growth.

The influence of capping agent on the morphologies was examined. Figure 4a, b exhibit SEM images of $CuFe_2O_4$ which achieved by sodium dodecyl solfate (as anionic surfactant) at 200 °C. The images show the size of mono-disperse particles is about 40 nm. Figure 4c, d exhibit SEM images of $CuFe_2O_4$ that achieved by SDS capping agent at 400 °C and approve particles are mono-disperse with average size about 50 nm.

Figure 5a, b show SEM images of the product achieved by poly-vinyl alcohol (as a green, cost-effective, biocompatible polymeric capping agent) at 200 °C which confirm formation of nanoparticles with mediocre size between 40 and 50 nm.

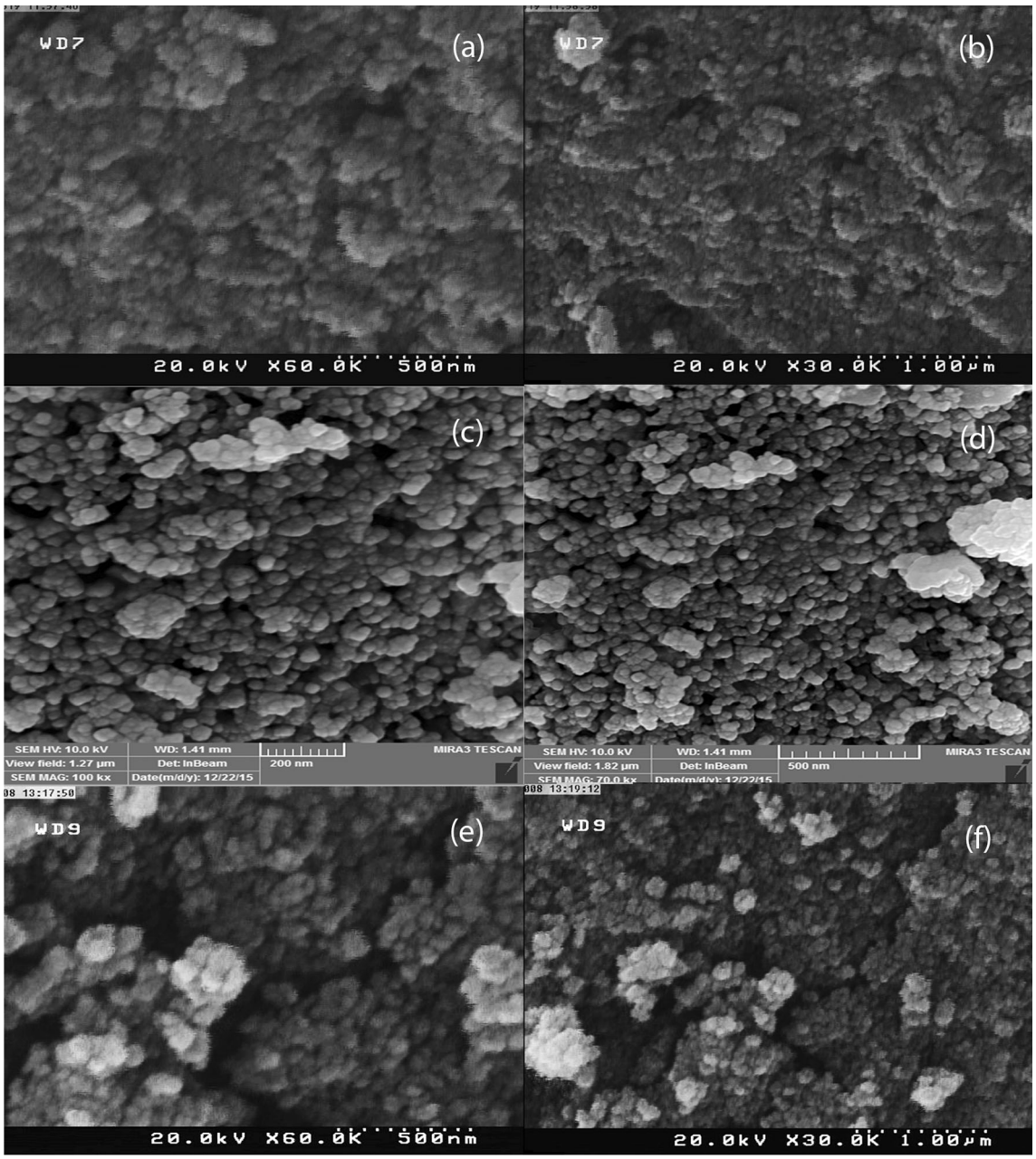

Fig. 5 SEM images of $CuFe_2O_4$ prepared by PVA **a**, **b** 200 °C no. 5; **c**, **d** 400 °C no. 6; **e**, **f** 600 °C no. 7

SEM images of the ferrites obtained by PVA (170,000) at 400 °C are illustrated in Fig. 5c, d which approve preparation of nanoparticles with average size of around 60 nm. Figure 5e, f depict SEM images of the obtained $CuFe_2O_4$ by PVA at 600 °C which show synthesis of nanoparticles with diameter size between 50 and 70 nm.

In order to investigate the effect of precipitating agent on product nanostructure, changing from sodium hydroxide to ammonia was also examined. Figure 6a, b show SEM images of product that achieved by ammonia as a replacement for sodium hydroxide (as a weaker precipitating agent), and confirm preparation of nanoparticles with average size of 40 nm. The balance between nucleation and growth rates (which determines size and morphology of particle) depends on precursor, time and capping agent Fig. 6c, d show SEM images of products that achieved by ammonia at presence of PVA and the results show preparation of 40 nm nanoparticles. SEM image of product that achieved by ammonia as precipitating agent and SDS as a surfactant approves fabrication of nanoparticles with

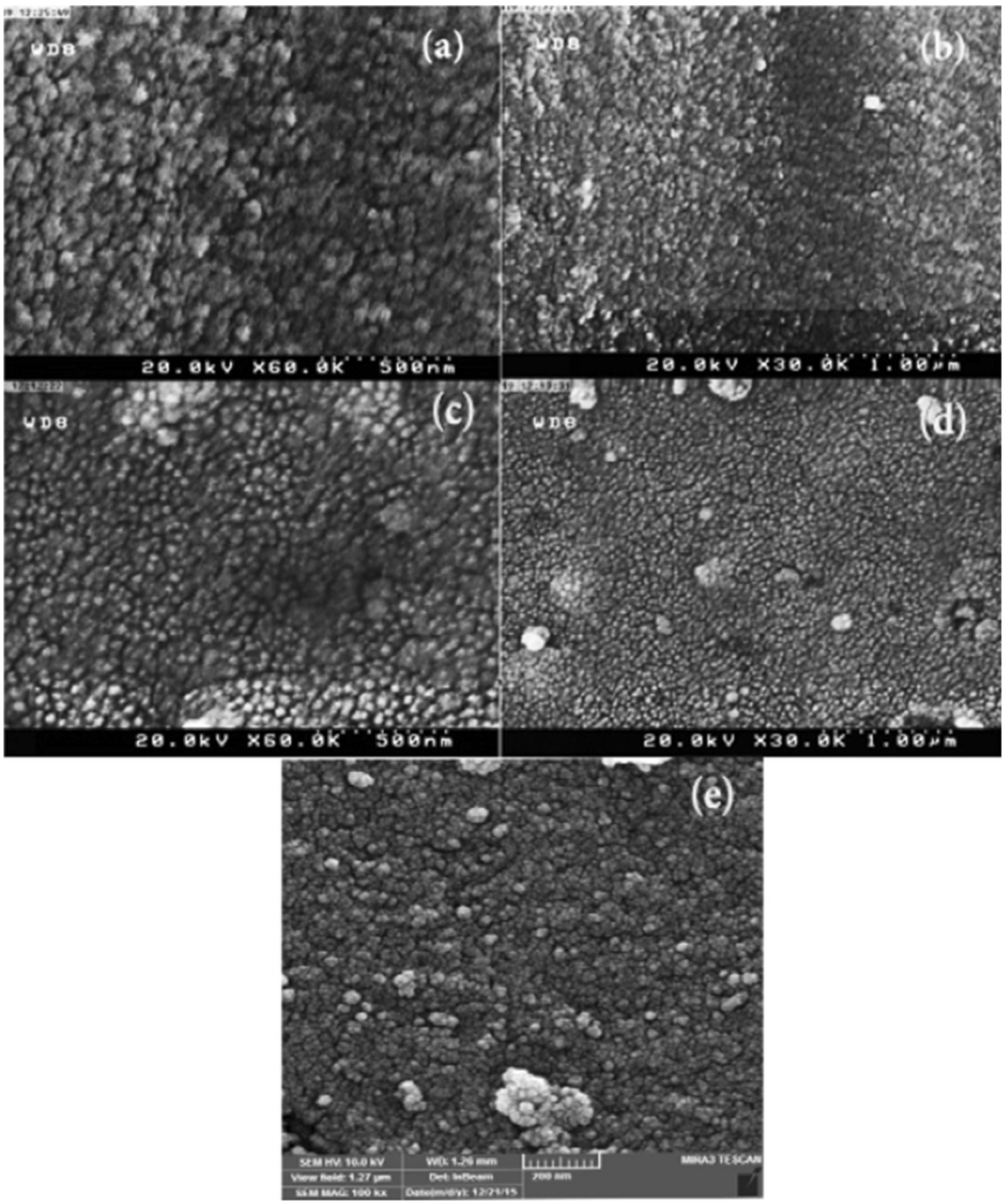

Fig. 6 SEM images of ferrite obtained by ammonia 200 °C **a**, **b** surfactant-free no. 8; **c**, **d** PVA no. 9; **e** SDS no. 10

average diameter size of about 50 nm (Fig. 6e). SEM images in two magnifications of the as-synthesized TiO_2 nanoparticles calcinated at 500 °C are presented in Fig. 7. As can be clearly seen the mono-dispersed photo-catalyst with size around 50 nm was synthesized in this condition.

The surfactant-free synthesized $CuFe_2O_4$ ferrites obtained at temperature of 200 °C was then composited by TiO_2 nanoparticles. SEM images of $CuFe_2O_4$–TiO_2 nanocomposite are shown in Fig. 8 at two magnifications. The images approve formation of mono-disperse structures with average particle size of around 50 nm.

Figure 9a shows the FT-IR spectrum of the as-prepared product with poly vinyl alcohol at 600 °C. The absorption bands at 433 and 600 cm^{-1} are assigned to the Fe–O and

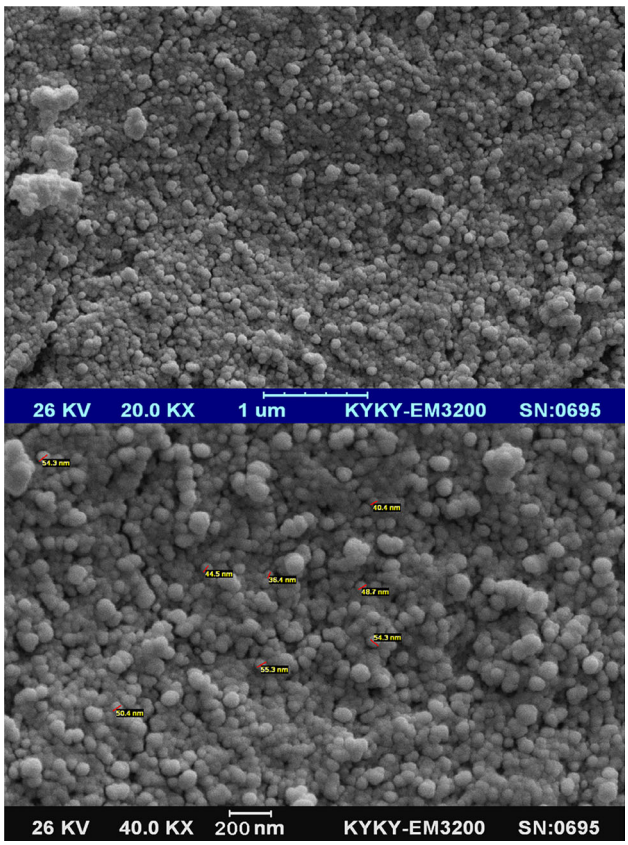

Fig. 7 SEM images of TiO_2 nanoparticles no. 11

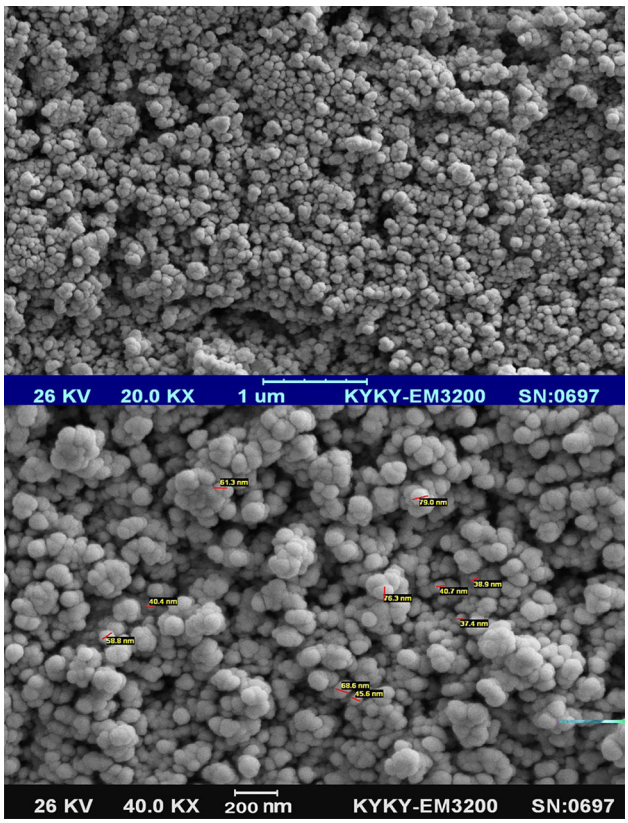

Fig. 8 SEM images of $CuFe_2O_4$–TiO_2 (50:50 %) nanocomposite no. 12

Cu–O (metal–oxygen bonds) stretching mode. The spectrum exhibits broad absorption a peak at 3411 cm^{-1}, corresponding to the stretching mode of O–H group of adsorbed hydroxyl group. Figure 9b shows the FT-IR spectrum of the as-prepared titanium dioxide. The absorption band at 758 cm^{-1} is assigned to the Ti–O (metal–oxygen bonds). Figure 9c shows the FT-IR spectrum of the as-prepared $CuFe_2O_4$–TiO_2 nanocomposite. It can be observed that the strong absorption bands at 583 and 758 cm^{-1} which are ascribed to phonon absorptions of the $CuFe_2O_4$–TiO_2 lattice and a broad absorption peak at 3419 cm^{-1} which is assigned to adsorbed O–H groups on the surface of nanoparticles. A weak band near 1623 cm^{-1} is observed which is assigned to H–O–H bending vibration mode due to the adsorption of moisture on the nanoparticles surface. There are no other significant peaks related to precursors and other impurities.

Room temperature magnetic properties of samples were studied using an AGFM instrument. Magnetization curve for $CuFe_2O_4$ nanoparticles is shown in Fig. 10. The curve indicates that the synthesized ferrite nanoparticles which annealed at 200 °C exhibits superparamagnetic behaviour with a zero coercivity and a magnetization of 1.8 emu/g when subjected to an applied magnetic field of 8000 Oe. Magnetization curve of magnetic $CuFe_2O_4$ nanoparticles which annealed at 400 °C is shown in Fig. 11. The curve indicates that this sample also exhibit show superparamagnetic behaviour with a magnetization of 2 emu/g (in an applied magnetic field of 8000 Oe) and zero coercivity. Hysteresis loop of magnetic $CuFe_2O_4$ nanoparticles, which annealed at 600 °C, is shown in Fig. 12. The sample exhibits ferromagnetic behaviour with a saturation magnetization of 25 emu/g and a coercivity of 587 emu/g. This sample has sufficient magnetizations which can simply be attracted by a laboratory magnet, making them appropriate for core of recyclable photocatalyst. These results indicate that annealing temperature has an important effect on magnetic properties of synthesized $CuFe_2O_4$ nanoparticles. The magnetic property of prepared $CuFe_2O_4$–TiO_2 nanocomposite was also investigated. The result shows superparamagnetic behaviour with a saturation magnetization of 0.95 emu/g and a coercivity of 3 emu/g (Fig. 13). This magnetization indicates that $CuFe_2O_4$–TiO_2 nanocomposites inherit the magnetic property from the $CuFe_2O_4$. However, the magnetization is lower due to presence of titanium dioxide. This reduction in saturation magnetization is due to the interfacial effect of the typical nanocomposite. The magnetic property of the prepared

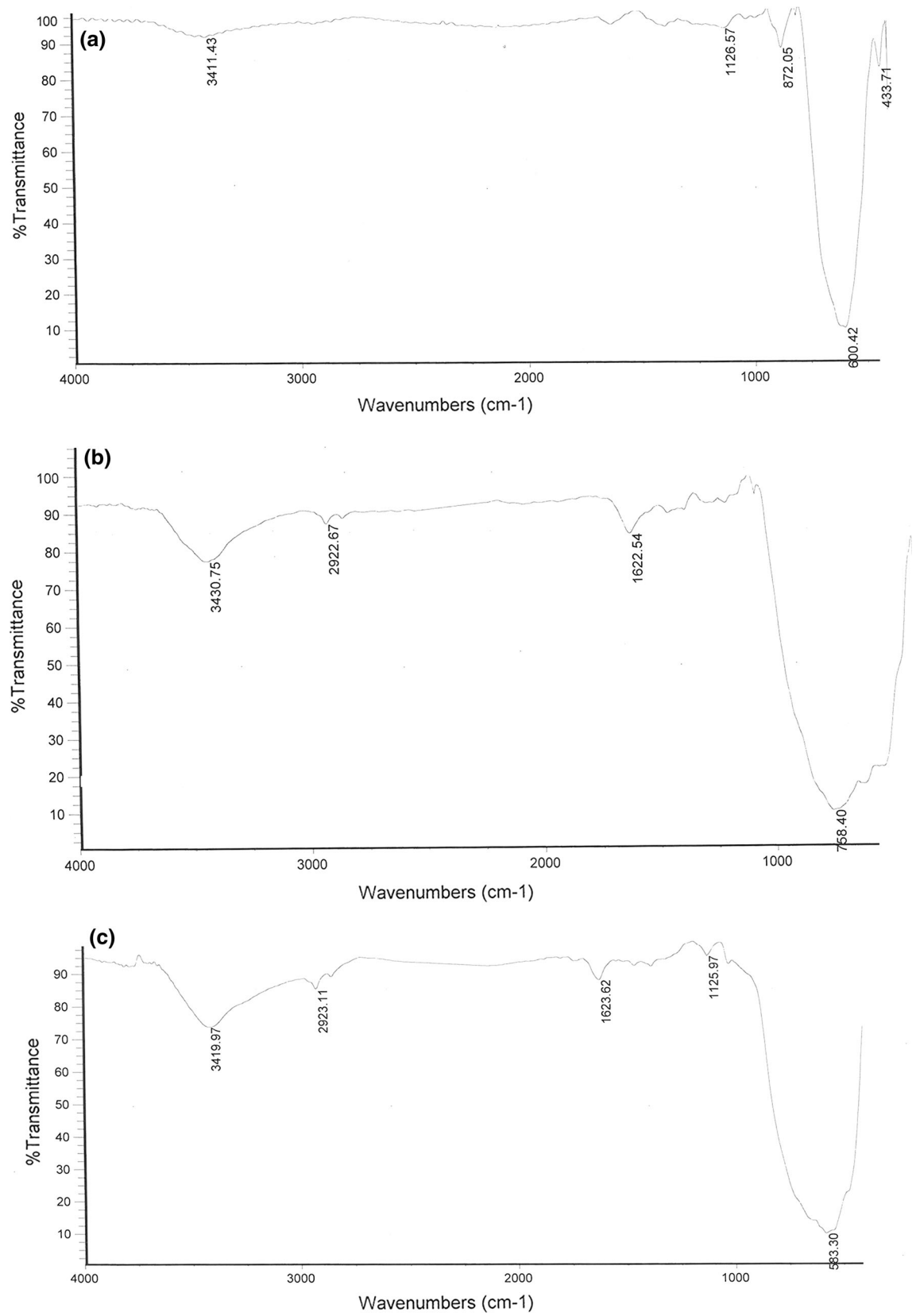

Fig. 9 FT-IR spectrum of **a** $CuFe_2O_4$ no. 7; **b** TiO_2 nanoparticles no. 11; **c** $CuFe_2O_4$–TiO_2 nanocomposite no. 12

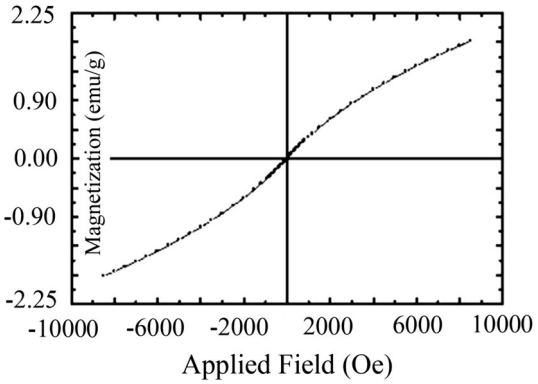

Fig. 10 Room temperature magnetization curve of $CuFe_2O_4$ nanoparticles no. 1 (200 °C)

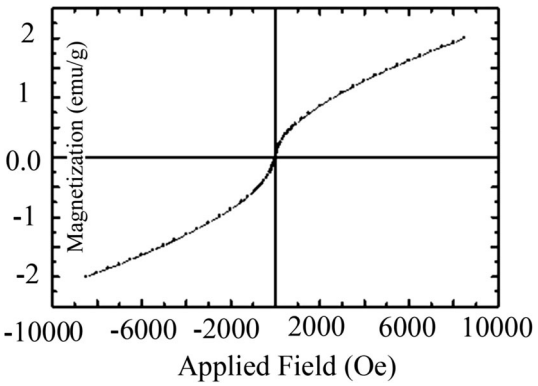

Fig. 11 Magnetization curve of $CuFe_2O_4$ nanoparticles (400 °C) no. 2

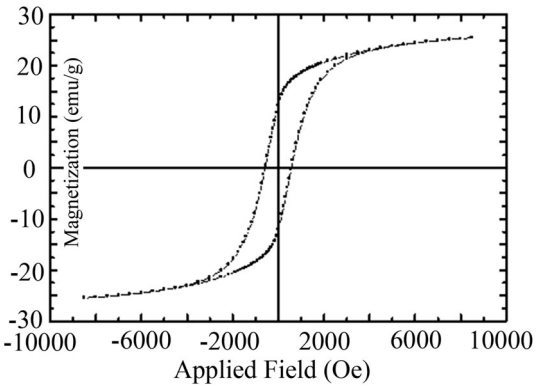

Fig. 12 Hysteresis loop of $CuFe_2O_4$ nanoparticles (600 °C) no. 7

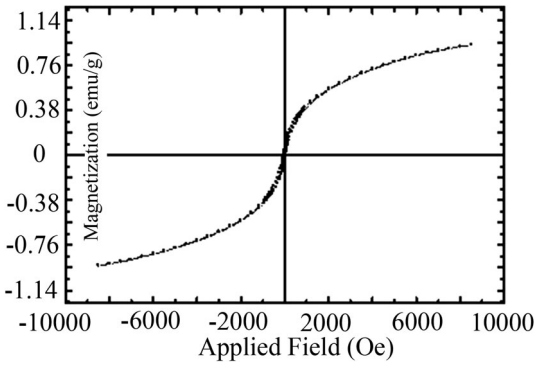

Fig. 13 Magnetization curve of $CuFe_2O_4$–TiO_2 nanocomposite (200 °C) no. 12

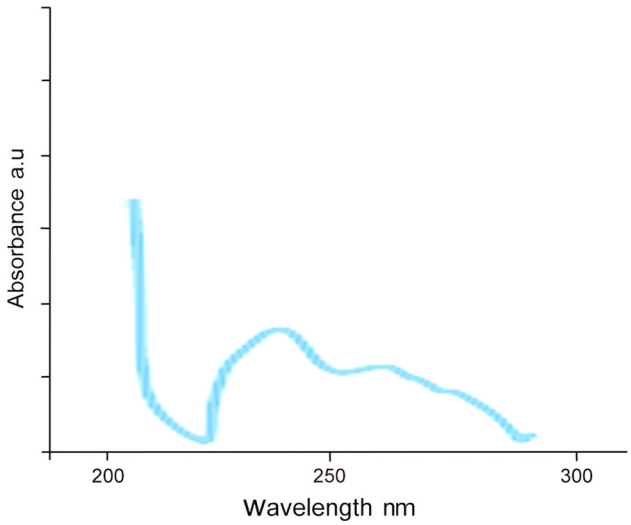

Fig. 14 UV–vis spectrum of TiO_2 nanoparticles no. 11

nanocomposites is an essential characteristic of a re-generable and re-usable magnetic heterogeneous catalyst.

The absorption spectrum of the titanium dioxide under UV–visible light was investigated and is depicted in Fig. 14. The photo-catalytic activity of the $CuFe_2O_4$–TiO_2 nanocomposite was evaluated by monitoring the degradation of four azo dyes in an aqueous solution, under irradiation of UV light. Chemical formulas of azo dyes acid black 1, acid blue 9, acid brown 14 and Congo red are shown in Fig. 15. The changes in the concentration of dye are illustrated in Figs. 16, 17, 18, 19. Acid black 1, acid blue 9, acid brown 14 and Congo red were degraded around 95, 80, 70 and 99 % at 60 min. Organic dyes decompose to

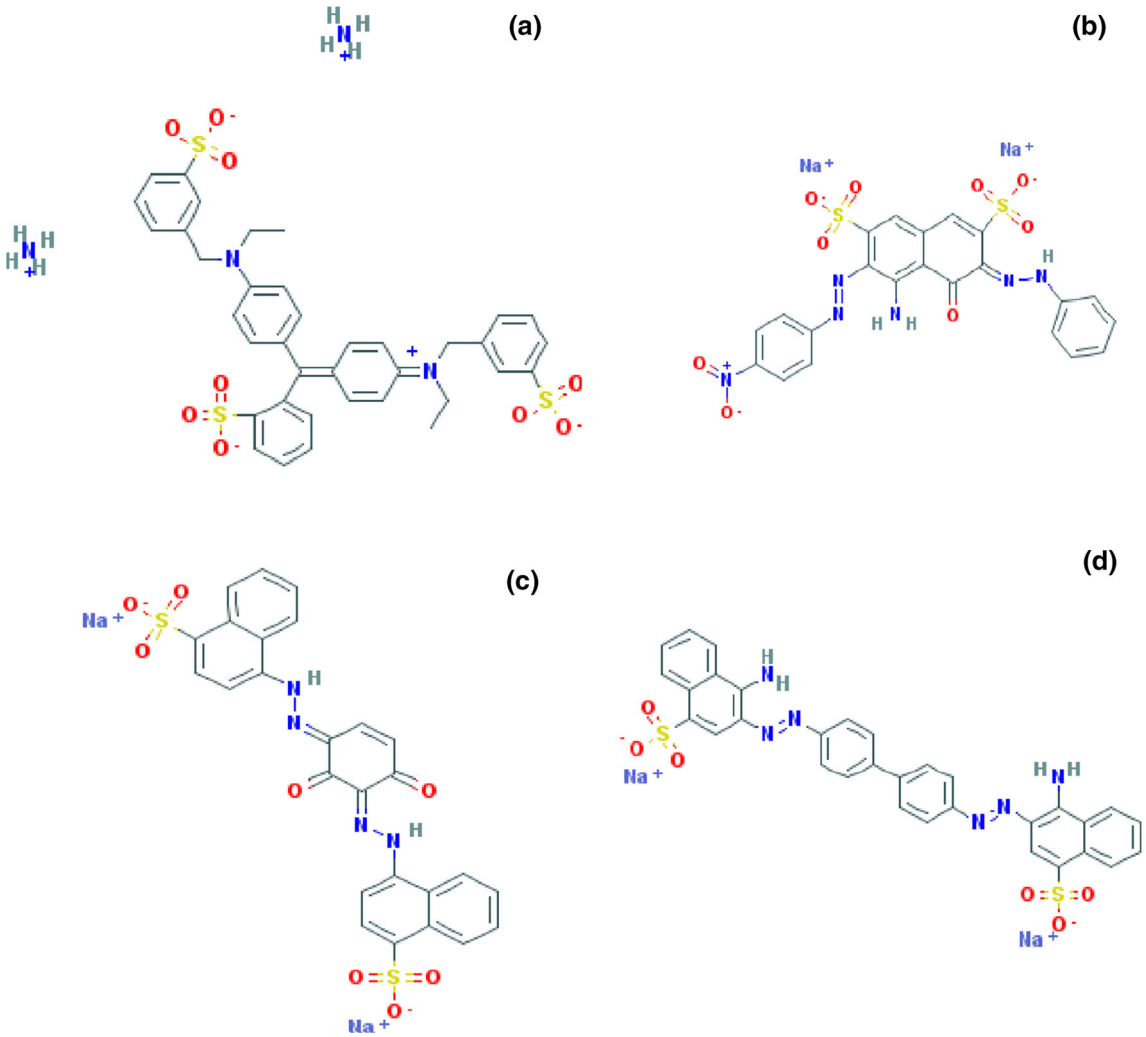

Fig. 15 Chemical formulas of azo dyes **a** acid *blue* 9, **b** acid *black* 1, **c** acid *brown* 14, **d** congo *red* (pH = 3) (Color figure online)

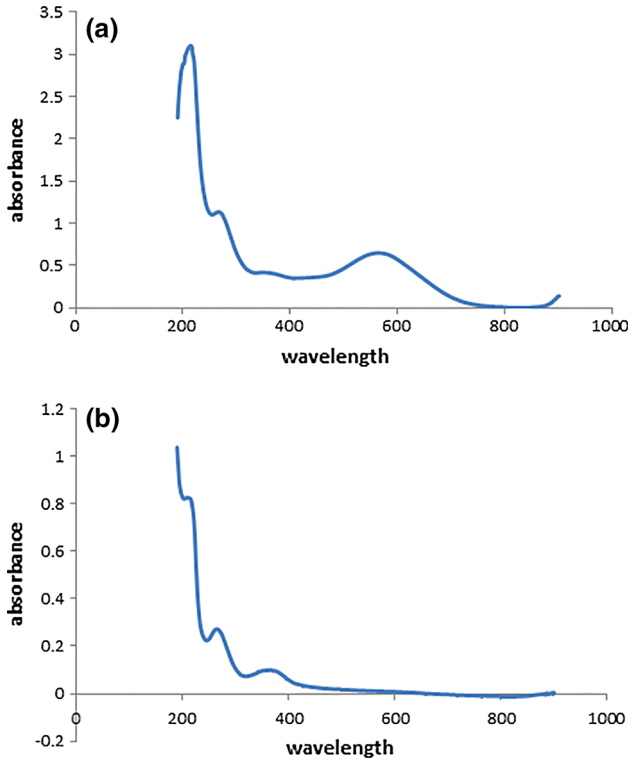

Fig. 16 Photo-degradation of acid black 1 **a** 0 min, **b** 60 min

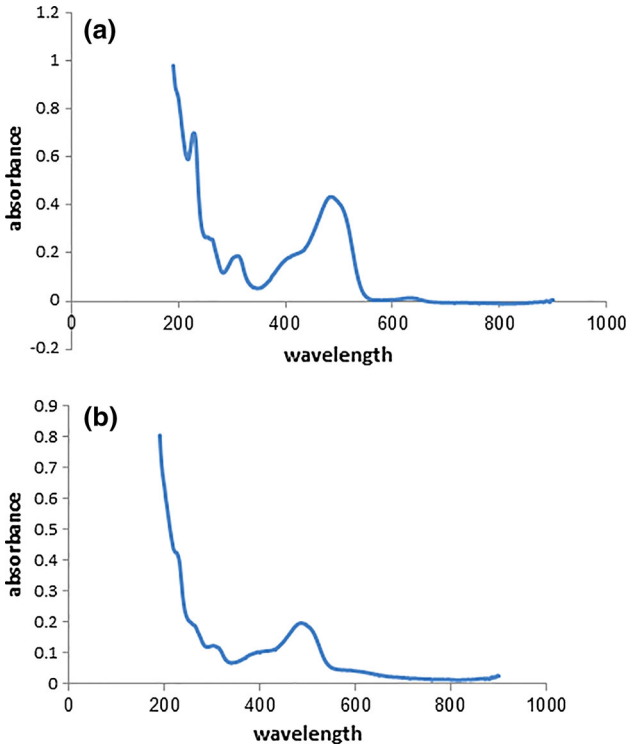

Fig. 18 UV–vis spectra of degradation of Acid *brown* 14, **a** 0 min, **b** 60 min (Color figure online)

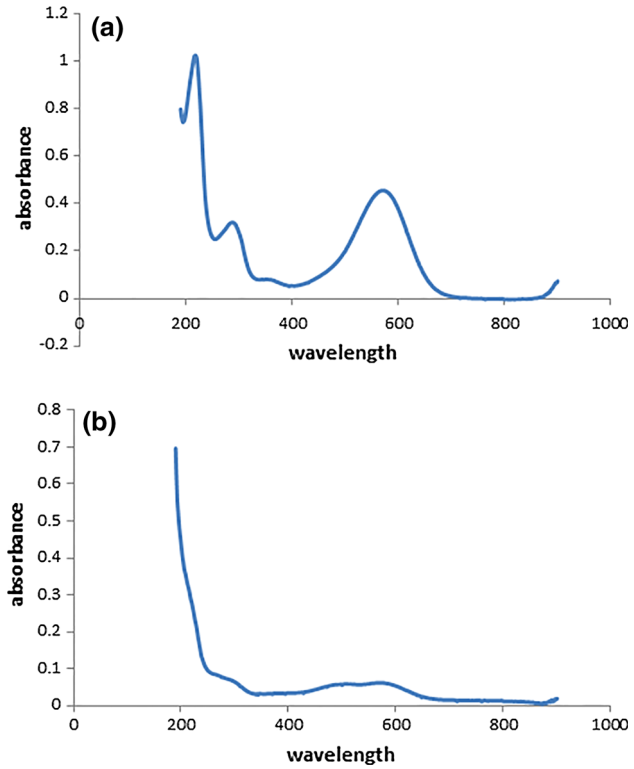

Fig. 17 UV–vis spectra of photo-degradation of acid *blue* 9, **a** 0 min, **b** 60 min (Color figure online)

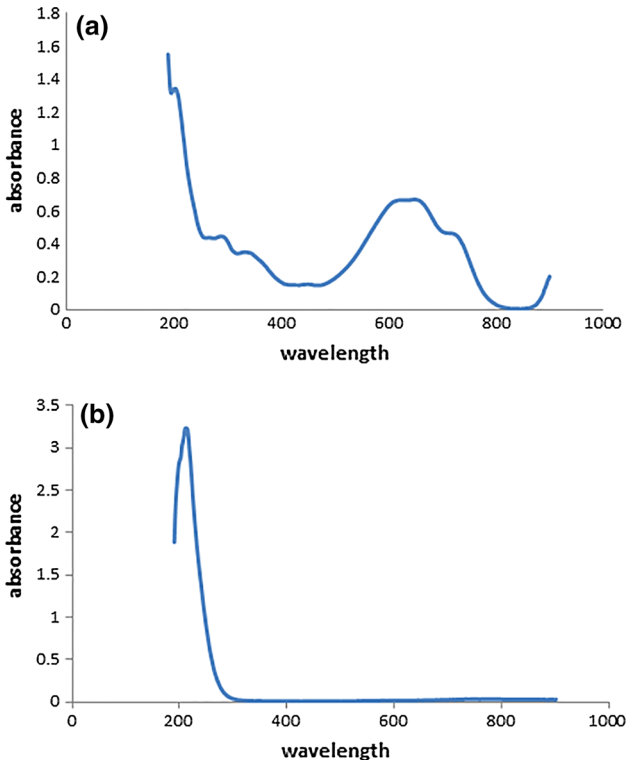

Fig. 19 Photo-degradation of congo *red* (pH = 3), **a** 0 min, **b** 60 min (Color figure online)

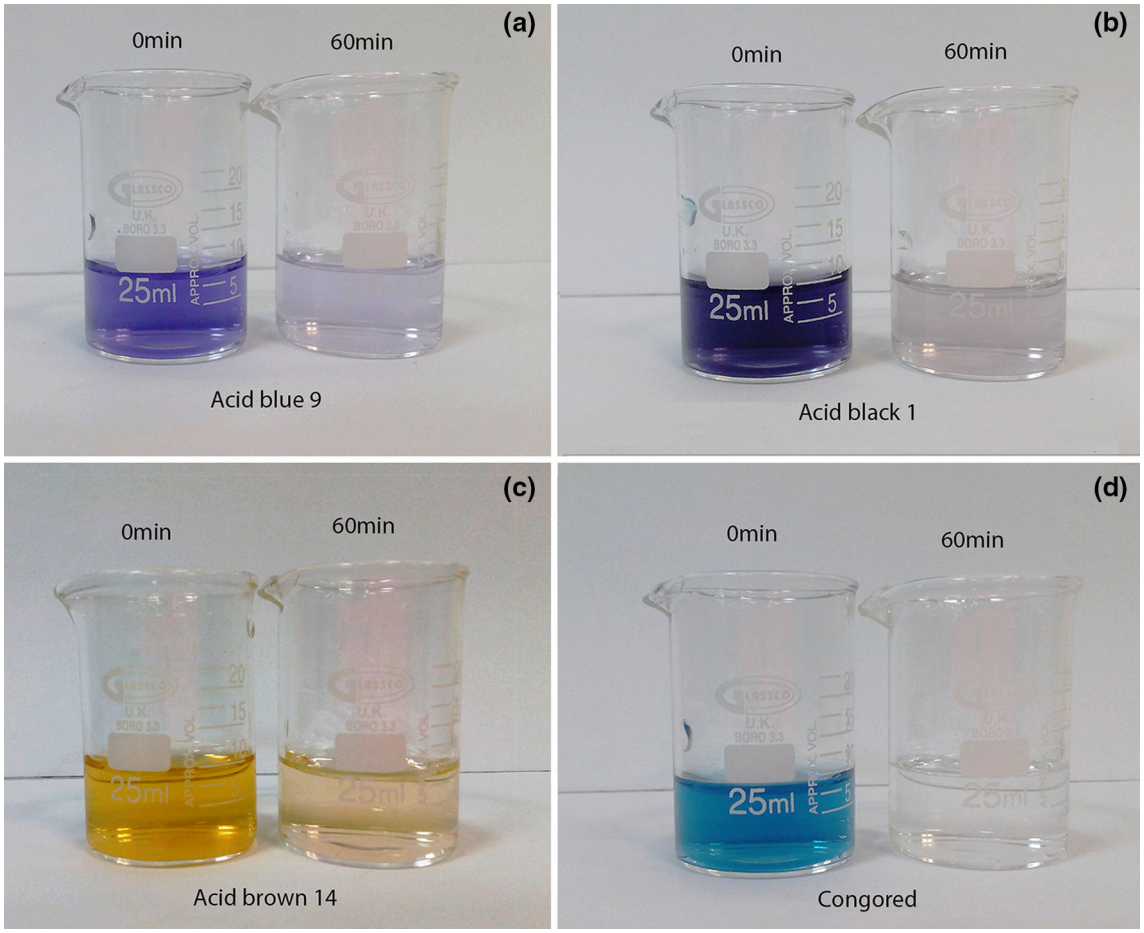

Fig. 20 Photocatalytic activity of $CuFe_2O_4$–TiO_2 nanocomposite

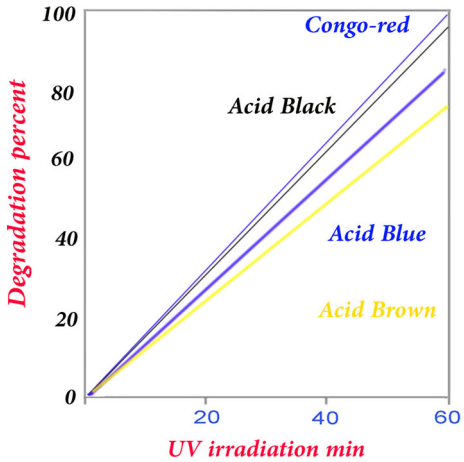

Fig. 21 Photo-degradation of azo-dyes

carbon dioxide, water and other less toxic or nontoxic residuals [21–24]. Figures 20 and 21 show degradation of four azo dyes after 60 min exposure to the $CuFe_2O_4$–TiO_2 nanocomposite.

4 Conclusions

Magnetic copper ferrite nanoparticles were synthesized via a simple precipitation method then $CuFe_2O_4$–TiO_2 nanocomposites were prepared via a simple sol–gel method. Effects of temperature and various surfactants on the morphology and particle size of the products were investigated. AGFM confirmed that nanocomposites exhibit either superparamagnetic or ferromagnetic behaviour. The photocatalytic behaviour of $CuFe_2O_4$–TiO_2 nanocomposite was evaluated using the degradation of four azo dyes under UV light irradiation. The results show that precipitation and sol–gel method are suitable method for preparation of $CuFe_2O_4$–TiO_2 nanocomposites as a candidate for photocatalytic applications.

Acknowledgments This work has been supported financially by Arak University Research Council (AURC) under the Grant number of 95-148 [95-2-13]. The authors acknowledge AURC for the financial support.

References

1. C. Munteanu, M. Caldararu, D. Gingasu, M. Feder, L. Diamandescu, N.I. Ionescu, React. Kinet. Mech. Catal. **104**, 357 (2011)
2. C. Reitz, C. Suchomski, J. Haetge, T. Leichtweiss, Z. Jaglicic, I. Djerdjc, T. Brezesinski, Chem. Commun. **48**, 4471 (2012)
3. G. Nabiyouni, D. Ghanbari, A. Yousofnejad, M. Seraj, Z. Mirdamadian, J. Nano Struct. **3**, 155 (2013)
4. A. Bagheri Ghomi, V. Ashayeri, Iran. J. Catal. **3**(3), 135 (2012)
5. G.R. Kumar, K.V. Kumar, Y.C. Venudhar, Mater. Sci. Appl. **3**, 87 (2012)
6. A. Goyal, S. Bansal, S. Singhal, Int. J. Hydrog. Energy **39**, 4895 (2014)
7. S. Singh, B.C. Yadav, V.D. Gupta, P.K. Dwivedi, Mater. Res. Bull. **47**, 3538 (2012)
8. J. Feng, L. Su, Y. Ma, C. Ren, Q. Guo, X. Chen, Chem. Eng. J. **221**, 16 (2013)
9. L.B. Zakiyah, E. Saion, N.M. Al-Hada, E. Gharibshahi, A. Salem, N. Soltani, S. Gene, Mater. Sci. Semicond. Process. **40**, 564 (2015)
10. W. Ponhan, S. Maensiri, Solid State Sci. **11**, 479 (2009)
11. R. Köferstein, T. Walther, D. Hesse, S.G. Ebbinghaus, J. Solid State Chem. **213**, 57 (2014)
12. M. Feng, A. Yang, X. Zuo, C. Vittoria, V.G. Harris, J. Appl. Phys. **09A521**, 107 (2010)
13. M.R. Uddin, M.R. Khan, M.W. Rahman, A. Yousuf, C.K. Cheng, React. Kinet. Mech. Cat. **116**, 589 (2015) doi:10.1007/s11144-015-0911-7
14. H. Yang, J. Yan, Z. Lu, X. Chenga, Y. Tanga, J. Alloys Compd. **476**, 715 (2009)
15. M.G. Naseri, E.B. Saion, H.A. Ahangar, A.H. Shaari, Mater. Res. Bull. **48**, 1439 (2013)
16. X. Zuo, J. Appl. Phys. **99**, 909 (2006)
17. M.J. Iqbal, N. Yaqub, B. Sepiol, B. Ismail, Mater. Res. Bull. **46**, 1837 (2011)
18. M.M. Rashad, R.M. Mohamed, M.A. Ibrahim, L.F.M. Ismaild, E.A. Abdel-Aal, Adv. Powder Technol. **23**, 315 (2012)
19. N.M. Deraz, J. Alloys Compds. **501**, 317 (2010)
20. M. Masjedi-Arani, M. Salavati-Niasari, D. Ghanbari, G. Nabiyouni, Ceram. Int. **40**, 495 (2014)
21. J. Saffari, N. Mir, D. Ghanbari, K. Khandan-Barani, A. Hassanabadi, M.R. Hosseini-Tabatabaei, J. Mater. Sci. Mater. Electron. **26**, 9591 (2015)
22. A. Esmaeili-Bafghi-Karimabad, D. Ghanbari, M. Salavati-Niasari, L. Nejati-Moghadam, S. Gholamrezaei, J. Mater. Sci. Mater. Electron. **26**, 6970 (2015)
23. M. Goudarzi, D. Ghanbari, M. Salavati-Niasari, A. Ahmadi, J. Clust. Sci. **27**, 25 (2016)
24. J. Saffari, H. Shams, D. Ghanbari, A. Esmaeili, J. Clust. Sci. **25**, 1225 (2014)
25. M. Fedailaine, S. Berkani, M. Trari, Korean J. Chem. Eng. **32**(4), 1 (2015)
26. A. Kezzim, N. Nasrallah, A. Abdi, M. Trari, Energy Convers. Manag. **52**, 2800 (2011)
27. M. Rahim, M.R. Khan, M. Wasikur, A. Yousuf, C.K. Cheng, React. Kinet. Mech. Catal. **116**, 589 (2015)